

Affordance-Aware Object Insertion via Mask-Aware Dual Diffusion

Jixuan He^{1,2,*} Wanhua Li^{1,*} Ye Liu^{1,3} Junsik Kim¹ Donglai Wei⁴ Hanspeter Pfister¹
¹Harvard University ²Cornell Tech ³The Hong Kong Polytechnic University ⁴Boston College

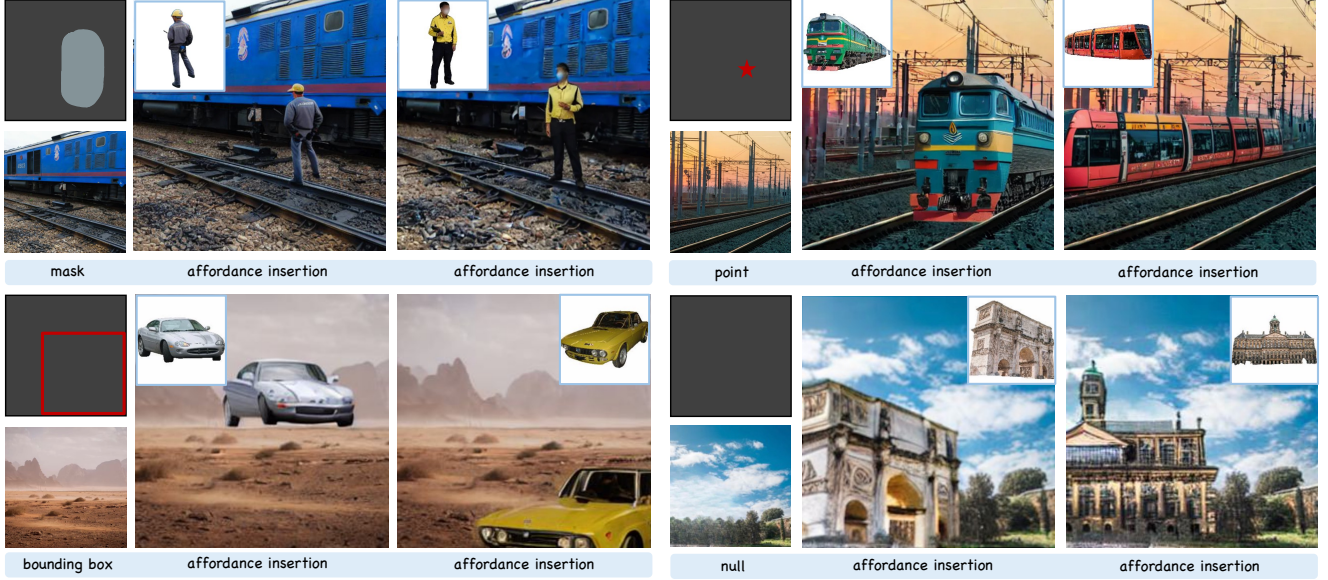


Figure 1. Given a foreground-background object-scene pair, our model can perform affordance-aware object insertion conditioning on different position prompts, including points, bounding boxes, masks, and even null prompts.

Abstract

As a common image editing operation, image composition involves integrating foreground objects into background scenes. In this paper, we expand the application of the concept of Affordance from human-centered image composition tasks to a more general object-scene composition framework, addressing the complex interplay between foreground objects and background scenes. Following the principle of Affordance, we define the affordance-aware object insertion task, which aims to seamlessly insert any object into any scene with various position prompts. To address the limited data issue and incorporate this task, we constructed the SAM-FB dataset, which contains over 3 million examples across more than 3,000 object categories. Furthermore, we propose the **Mask-Aware Dual Diffusion (MADD)** model, which utilizes a dual-stream architecture to simultaneously denoise the RGB image and the insertion mask. By explic-

itly modeling the insertion mask in the diffusion process, MADD effectively facilitates the notion of affordance. Extensive experimental results show that our method outperforms the state-of-the-art methods and exhibits strong generalization performance on in-the-wild images. Please refer to our code on <https://github.com/KaKituken/affordance-aware-any>.

1. Introduction

In the image composition scenario, common sense guides our perception of the authenticity of synthesized images: a person cannot levitate, a water bottle needs a surface for support, and a boat should be floating in the water rather than on the ground. Deviation from such common sense often leads to semantic inconsistencies in synthesized images. From a composition perspective, the background’s semantic richness plays a pivotal role in defining the placement and characteristics of foreground objects. To better describe the

*Equal Contribution.

†Work done while at Harvard University.

influence of background semantics on the foreground, we borrow the concept of *affordance* into object-scene composition tasks. Previously, Kulal *et al.* [24] explored the concept of human affordance for image synthesis. Their work, focused on inserting humans into masked scenes, extends beyond mere color or view adjustments. To generalize the setting to arbitrary object-scene synthesis, we term the new task *Affordance-Aware Object Insertion*. This task challenges models to identify suitable locations and make necessary adjustments to foreground objects, ensuring the generated images adhere to physical laws.

This work aims to build a foundation model for affordance-aware object insertion, which can put any object into any scene as shown in Figure 1. There are three primary challenges involved. First, the model must accurately recognize the appropriate affordance relationship between a background and the foreground object to be inserted. Adjustments to the inserted foreground object are crucial for achieving the intended semantic consistency. The second challenge lies in the model’s ability to generalize across a diverse range of foreground objects. Previous generative image editing methods, such as textual inversion [11], DreamBooth [40], and DreamEdit [26], are subject-specific thus hard to generalize. Our goal is to train a model that can generalize to any object. Third, our model should support a variety of input prompts for users to specify insertion locations, ranging from sparse formats like points and bounding boxes to dense masks. Moreover, in the absence of explicit prompts, the model can autonomously determine appropriate insertion locations by analyzing the semantic content of both the background and foreground.

We address these challenges through three components: **task**, **data**, and **model**. Extending the concept of *affordance* beyond Kulal *et al.*’s initial scope [24], the task of affordance-aware object insertion aims to place an arbitrary object into any scene, accommodating different positional prompts, even in the absence of explicit positional cues. It has significant implications for applications such as automated dataset synthesis. To support this task, a large-scale dataset is necessary. Existing image composition datasets, such as DreamEditBench [26], are limited in terms of the diversity of foreground object categories and the number of training samples. To overcome these limitations, we curate a new dataset called SAM-FB which is derived from SA-1B [23] for affordance learning. SAM-FB contains a variety of foreground object categories and over 3 million samples. With SAM-FB, we further propose a **Mask-Aware Dual Diffusion (MADD)** model to utilize the large-scale data, which is a diffusion-based framework that facilitates the seamless integration of diverse objects into any scene. During the denoising procedure, object position is progressively refined while the target RGB image is synthesized simultaneously, ensuring accurate alignment between objects

and positions to achieve affordance-aware insertion. Furthermore, we present a unified representation for sparse and dense prompts, enabling our model to interpret and respond to various types of position inputs effectively.

The contributions of this work are as follows:

- We formulate the task of affordance-aware object insertion, which extends general object-scene composition with affordance guidance, aiming to achieve realistic object insertion with diverse prompts.
- We introduce SAM-FB, a large-scale dataset with diverse object categories for affordance-aware object insertion, which consists of over 3 million samples.
- To facilitate the learning of the affordance concept, we propose the mask-aware dual diffusion model, which adopts a dual-stream architecture to simultaneously denoise the appearance and the insertion mask.

2. Related Work

Affordance. J.J. Gibson [3] first introduces the concept of affordance, then a series of papers [4, 10, 14, 28] dug into this concept and brought it into the image synthesis. Initially grounded in psychology, the concept emphasizes that an object’s appearance should correspond with its utilitarian aspects as perceived by humans. Further exploration within the field of image synthesis involved adjusting the orientation and gestures of generated human figures to align with their background. Therefore, prior work primarily focuses on the interaction between humans and objects [12, 49, 52] or the human-scene relationship [7, 9, 46]. Kulal *et al.* [24] made progress by introducing a model trained on person movement video data for placing people within scenes and adjusting its pose according to the surroundings. However, their model’s scope was limited to human figures. Despite these advancements, the concept of “affordance” in image composition, which encompasses the positioning, viewing angle, and color harmony of objects within scenes, has remained relatively unexplored. Our work offers a generalised and versatile solution for object-scene composition.

Image Editing. Image editing aims to modify existing images using generative models. Generally, image editing can be divided into semantic editing (*e.g.* adding or removing objects, changing the background), style editing (*e.g.* altering color or texture), and structural editing (*e.g.* changing object size or viewpoint). By utilizing generative models like GANs [13] or Diffusion [8], users can edit image content by providing instructions and multi-modal prompts. For instance, InstructPix2Pix [5] and MoEController [25] allow semantic and style editing through text-based instructions provided by users, while Imagen Editor [45] enables more precise control of edit locations by accepting user-provided masks for the areas to be edited. Additionally, other image editing models, such as TF-ICON [33] and Im-

Dataset	Sample No.	Category No.
DreamEditBench	440	22
MureCom	640	32
SAM-FB (Ours)	3,160,403	3,439

Table 1. Dataset comparison. Our dataset contains significantly more training samples and object categories.

ageBrush [48], accept reference images from users, constraining the appearance of objects during editing.

Image Composition. Image composition is a sub-task within image editing, primarily focused on controllably inserting foreground objects into a background based on reference images. Recently, the utilization of generative models empowers high-quality and controllable image composition. Diffusion models have been successfully applied in various domains, including image composition [31, 42], video generation [18], and data augmentation [44]. Stable Diffusion (SD) [39] introduced methods for blending feature and semantic information from images and text, enabling object generation based on prompt instructions. Inpainting [2] is a common approach to achieve image composition. SD-based inpainting models [27, 34, 50] allow users to repaint a specific region with a mask, but it’s hard to insert a desired object into that region. Blended Diffusion [1] enables finer control by leveraging text descriptions of the foreground, but it’s crucial for user to describe the foreground precisely. PBE [47], ObjectStitch [42], and GLI-GEN [29] utilize reference images to incorporate rich visual information, achieving better perspective and color harmony. However, these models require users to provide precise positional cues, such as bounding boxes or masks, to indicate the insertion location. Our proposed method offers a viable solution for handling vague positional information, such as point prompts or even blank prompts.

3. Dataset

We constructed the **SAM-FB** benchmark dataset for the affordance-aware object insertion task.

Design Decisions. We designed the dataset to have: 1) Sufficient training samples. 2) A wide variety of foreground objects. 3) Well-aligned input-output pairs such as (f, b, p, x) tuples, where f , b , p , and x represent the foreground image, background image, position prompt, and ground truth image, respectively. Unfortunately, there is no existing dataset that meets the aforementioned requirements. As shown in Table 1, existing datasets such as DreamEditBench [26] and MureCom [32] contain only a very limited number of samples and object categories.

Our dataset is built upon the SA-1B [23] dataset to ensure a diverse category of foreground objects. SA-1B

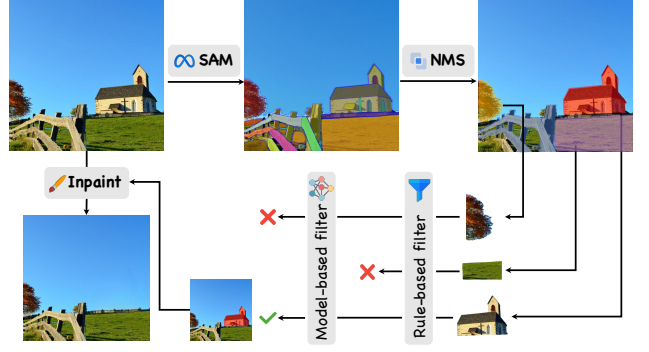


Figure 2. Pipeline of constructing the SAM-FB dataset. The background is inpainted and high-quality foreground objects are preserved through a data quality control stage.

contains 11 million high-quality images collected from all kinds of reality scenes and 1 billion well-annotated class-agnostic masks. We masked out the foreground object and inpainted the mask to obtain the background. The ground truth is the original image. To automate the process and improve the dataset quality, a scalable automatic annotation pipeline, and a data quality control are proposed. In the end, we obtain over 3 million well-annotated training samples organized in (f, b, p, x) format, where p consists of diverse position prompts generated from foreground masks.

Scalable Automatic Annotation Pipeline. As shown in Figure 2, the pipeline generates foreground-background pairs from images in the SA-1B dataset. For each input image, we first run SAM to obtain object masks as candidates. We then perform the Non-Maximum Suppression (NMS) with a high threshold (0.6) to deduplicate these masks. With these masks, we crop the objects to form the foreground f , and the remaining content is inpainted with LAMA [43] to create the background b . To ensure the inpainting quality of the background, we expand the boundaries of the object mask to avoid residual foreground content in the background following GroundingSAM [30, 38]. The original image serves as the ground truth x . The binary object mask is designated as m and we can derive multiple different positions prompts p such as point, bounding boxes using it, so that compose the input-output pairs (f, b, p, x) . This pipeline is scalable and no manual annotations are required in this process. With this pipeline, it’s feasible and easy for users to further scale up the SAM-FB dataset or customize their datasets with new source images.

Data Quality Control. We only keep high-quality foregrounds, since we may obtain masks that include unintended elements due to challenges in controlling the granularity and semantics of the segmentation while using SAM. They typically suffer from three issues: 1) Incompleteness. Some objects are obscured by others, resulting in only a small part of the original objects being visible. 2) Back-

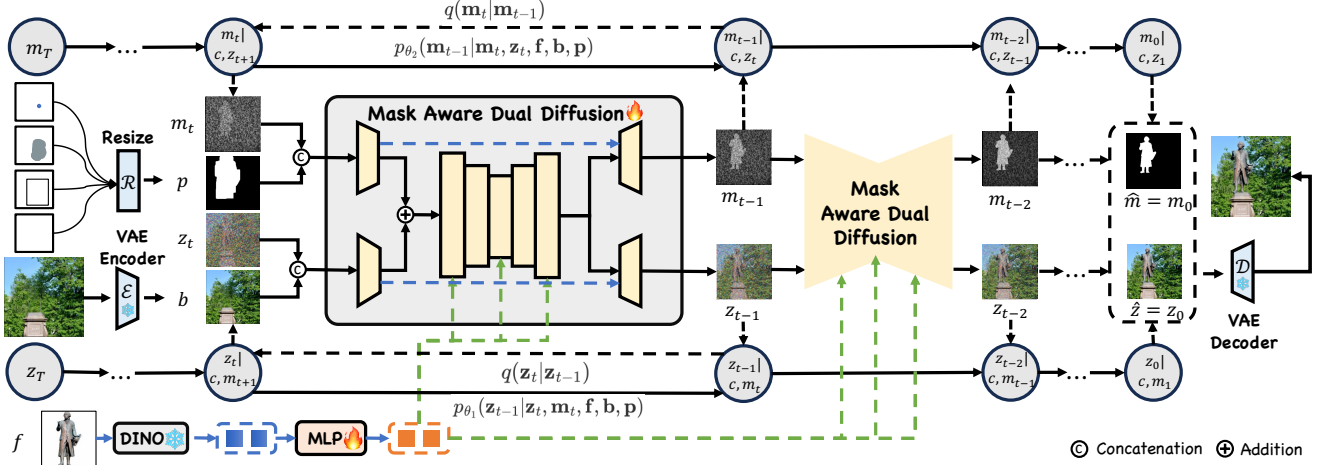


Figure 3. The framework of MADD. Foreground objects are encoded using a DINOv2 encoder, serving as the guidance signal through the cross-attention mechanism. The position prompt encoder unifies different types of position prompts, which are then concatenated with the latent mask \mathbf{m}_t . The background is encoded using a VAE encoder and then concatenated with the latent image \mathbf{z}_t . We use a dual branch structure to denoise RGB image \mathbf{z} and object mask \mathbf{m} simultaneously.

ground Masks. It is also possible to get some background masks such as a piece of sky or a coast, which cannot be treated as a foreground object. 3) Undersized Objects. Some tiny objects feature blurry details, thereby reducing data quality. To achieve quality control, we employ a combination of rule-based and learning-based methods to filter the foreground. We first filter masks by setting rules on their basic attributes. Then, we further employ a deep neural network to filter out low-quality objects. We annotate 2,000 foreground images with binary labels (*good* and *bad*) and fine-tune a pre-trained ResNet-50 [15] on those manually annotated images. The model is then able to assess the quality of the foreground. After the strict quality control, only 0.25% of the masks are left. Samples of low-quality objects and details of the filters are in the supplementary.

To justify the diversity of our proposed dataset, we use RAM [51] to recognize the categories of foregrounds we keep. We have identified 3439 different categories, which is a vast improvement over previous datasets. The word cloud of categories is shown in our supplementary.

4. Method

4.1. Task Formulation

We formally define the affordance-aware object insertion problem as follows: given a foreground object \mathbf{f} , a background scene \mathbf{b} , and a position prompt \mathbf{p} , the model \mathcal{G} is required to predict a synthesized image $\hat{\mathbf{x}}$ that places the object into the scene following the correct affordances and aligns with the intentions of the position prompt:

$$\hat{\mathbf{x}} = \mathcal{G}(\mathbf{f}, \mathbf{b}, \mathbf{p}). \quad (1)$$

The model must support flexible prompts \mathbf{p} , which include points, bounding boxes, masks, and even null prompts.

4.2. Mask-Aware Dual Diffusion

Inspired by the recent success of diffusion models [39], we adopt SD as the backbone of our model to achieve high-quality image synthesis. SD with condition guidance represents a Markov process where Gaussian noise $\epsilon_t \sim \mathcal{N}(0, 1)$ is added to the ground truth \mathbf{z}_0 to produce $\mathbf{z}_t = \alpha_t \mathbf{z}_0 + \sigma_t \epsilon_t$. Here, α_t and σ_t are scalars sampled by different samplers such as DDIM [41] and DDPM [17]. The objective of the SD is to reconstruct the reverse process $p_\theta(\mathbf{z}_0 | \mathbf{c})$:

$$p_\theta(\mathbf{z}_{0:T} | \mathbf{c}) = p(\mathbf{z}_T) \prod_{t=1}^T p_\theta(\mathbf{z}_{t-1} | \mathbf{z}_t, \mathbf{c}), \quad (2)$$

where \mathbf{c} is the condition to guide the denoising process. In our task, $\mathbf{z}_0 = \mathbf{x}$ and \mathbf{c} consists of a foreground image \mathbf{f} , a background image \mathbf{b} , and a position prompt \mathbf{p} .

For affordance-aware object insertion, one key goal is to determine an appropriate location and size for the object to be inserted. The final inserted region, *e.g.*, the insertion mask \mathbf{s} contains the accurate location, size, and shape information, yet hasn't been explicitly modeled in Eq. 2. To facilitate the learning of the affordance concept, we explicitly model the insertion mask \mathbf{s} in the diffusion process. Specifically, we propose a Mask-Aware Dual Diffusion model, which adopts a dual-stream architecture to simultaneously denoise the appearance and the insertion mask. Instead of just predicting the composed image, MADD also predicts the precise mask $\hat{\mathbf{m}}$ of the desired inserted object explicitly at each time step. This means that

the reverse process of \mathbf{m}_t and \mathbf{z}_t also depends on each other, so we have $p_\theta(\mathbf{z}_{t-1}|\mathbf{z}_t, \mathbf{m}_t, \mathbf{f}, \mathbf{b}, \mathbf{p})$ for the RGB stream and $p_\theta(\mathbf{m}_{t-1}|\mathbf{m}_t, \mathbf{z}_t, \mathbf{f}, \mathbf{b}, \mathbf{p})$ for the mask stream, where $\mathbf{m}_t = \alpha_t \mathbf{m}_0 + \sigma_t \epsilon_t^m$, $\epsilon_t^m \sim \mathcal{N}(0, 1)$, and $\mathbf{m}_0 = \mathbf{s}$. Note that although \mathbf{s} is included in our SAM-FB dataset, it can be directly derived from the difference between the ground truth \mathbf{x} and the background \mathbf{b} .

For the diffusion process of MADD, we have

$$\begin{aligned} p_{\theta_1}(\mathbf{z}_{0:T}|\mathbf{c}, \mathbf{m}_{0:T}) &= p(\mathbf{z}_T) \prod_{t=1}^T p_{\theta_1}(\mathbf{z}_{t-1}|\mathbf{z}_t, \mathbf{m}_t, \mathbf{c}) \\ p_{\theta_2}(\mathbf{m}_{0:T}|\mathbf{c}, \mathbf{z}_{0:T}) &= p(\mathbf{m}_T) \prod_{t=1}^T p_{\theta_2}(\mathbf{m}_{t-1}|\mathbf{z}_t, \mathbf{m}_t, \mathbf{c}), \end{aligned} \quad (3)$$

where θ_1 and θ_2 represents parameters for different tasks: $\theta_i = \theta_{shared} \cup \theta_{expertise}^i$. Every time step, the denoiser ϵ_θ takes the foreground, background, position prompt, and time step t as input to predict the noise map ϵ_t for the RGB image and ϵ_t^m for the mask as follows:

$$\epsilon_t, \epsilon_t^m = \epsilon_\theta(\alpha_t \mathbf{z}_0 + \sigma_t \epsilon_t, \alpha_t \mathbf{m}_0 + \sigma_t \epsilon_t^m, \mathbf{c}). \quad (4)$$

Figure 3 shows the framework of the MADD. Inspired by Liu *et al.* [31], we utilize a single UNet with two expert input-output branches to denoise them simultaneously. The two tasks share the entire UNet except for the `conv_in`, first Down Block, last Up Block, and the `conv_out`. These independent blocks serve as the expertise input-output branch. Skip connection is also performed between the corresponding expertise input and output branches. This dual diffusion architecture reuses most of the parameters, encouraging the model to incorporate knowledge from two relevant tasks.

Modeling p_{θ_1} and p_{θ_2} is equivalent to estimating the noise terms ϵ_t and ϵ_t^m at each time step. This can be achieved by minimizing the loss function for RGB images and insertion masks:

$$\mathcal{L}_z(\theta_1) = \mathbb{E} [w_t \|\epsilon_t - \epsilon_\theta(\alpha_t \mathbf{z}_0 + \sigma_t \epsilon_t; t, \mathbf{m}_t, \mathbf{c})\|^2] \quad (5)$$

$$\mathcal{L}_m(\theta_2) = \mathbb{E} [w_t \|\epsilon_t^m - \epsilon_\theta(\alpha_t \mathbf{m}_0 + \sigma_t \epsilon_t^m; t, \mathbf{z}_t, \mathbf{c})\|^2] \quad (6)$$

w_t is a function weighing the contributions of denoising tasks to the training objective, commonly set to 1. During the training procedure, the time step t is sampled from a uniform distribution $\mathcal{U}[0, 1]$. The final loss function for MADD is obtained by combining the above losses:

$$\mathcal{L}(\theta) = \mathcal{L}_z(\theta_1) + \mathcal{L}_m(\theta_2). \quad (7)$$

4.3. Affordance Condition

Foreground Encoder. In MADD, foreground images serve as a guidance condition and are injected into the main-stream using cross-attention. The foreground embedding

can be any tokenized features obtained by a ViT-like visual encoder. In SD, the CLIP [37] encoder is used to provide text semantics for cross-attention. Following Efficient-3DiM [20], we use DINOv2 [35] as the encoder. While CLIP visual features are designed to align with textual features, typically encapsulating high-level semantic features, DINOv2 features preserve detailed object information, which is crucial for our task.

Background Encoder. Following practices in SD-based image editing methods [5, 42], we use a frozen pre-trained VAE Encoder to encode the background image to a 4-channel latent map. As the background image is pixel-aligned with the output, we concatenate the background latent map with the \mathbf{z}_t and send them to the UNet. The pre-trained VAE decoder is then used to transform the latent output back to RGB space.

Position Prompt Encoder. To accommodate various position prompts, we have designed a unified representation that processes different types of prompts. Specifically, we convert both sparse and dense position prompts into a unified dense representation. Each type of prompt is represented as a 1-channel position map. Note that these position prompts serve as rough guides for the placement of foreground objects, therefore we consider building a probability map for the 1-channel position map. For point prompts, we transform them into a Gaussian heatmap where the point is positioned at the center of the Gaussian. When dealing with bounding box prompts, we fill the area inside the box with ones and the outside with zeros. For mask prompts, we set the values inside the mask to 1 and all other values to 0. For the null prompt, we use an all-one image, implying that all positions are possible. Subsequently, we resize the position map to match the spatial dimensions of the latent map \mathbf{m}_t , and concatenate it with \mathbf{m}_t along the channel dimension before feeding it into the diffusion U-Net.

4.4. Implementation Details

To leverage prior knowledge of real-world images, we initialize our model with a pre-trained Stable Diffusion In-painting model for the neural layers with the same configuration. Fine-tuning a diffusion model is resource-consuming, but we can make it more efficient using the feature that the model is image-size unaware. Therefore, we first train the model on 128×128 resolution to accelerate training, with a batch size of 1024 on 2 A-100 GPUs for 35K steps. We then fine-tune it on 256×256 resolution with a batch size of 256 for 15K steps. For each foreground object, all different position prompts \mathbf{p} can be generated with the mask \mathbf{s} . During training, we randomly selected one of the position prompts as input with equal probability. We use Classifier-Free Guidance [16] to improve the insertion quality. During training, we drop all the conditions with a probability of 0.1 and only drop \mathbf{p} with a probability of

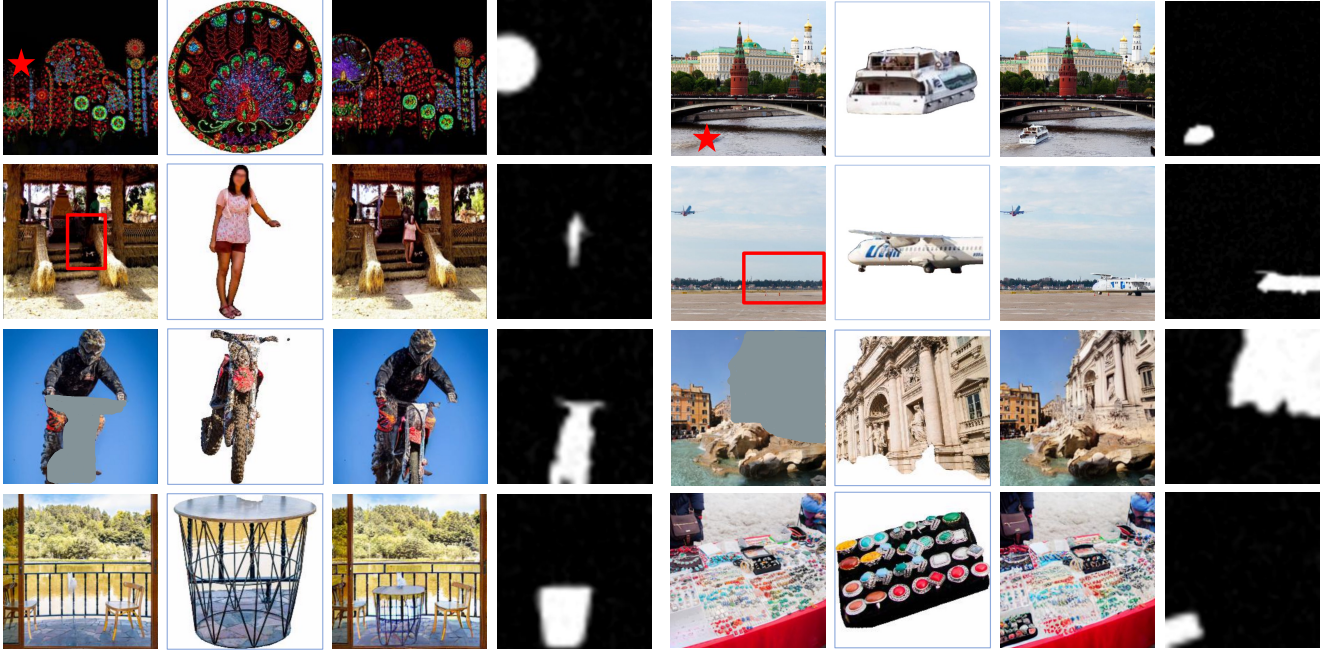


Figure 4. Qualitative results of MADD on the SAM-FB test set. Each row corresponds to one type of prompt, *i.e.*, point, bounding box, mask, and null, respectively. Our MADD simultaneously predicts the RGB image and the object mask.

0.1. We also perform strong data augmentation to both foreground images and position prompts to prevent the model from learning a mere copy-and-paste process. Please refer to the supplementary for details.

5. Experiments

5.1. Results on the SAM-FB Test Set

Evaluation Metrics. Following the previous work [6, 19, 22, 33], we employ the FID score to measure the quality of images obtained by generative models and the CLIP score to evaluate the semantic similarity between the edited region and the reference foreground.

Quantitative Comparison. We compare our method with Stable Diffusion [39], PBE [47], GLI-GEN [29], and Human Affordance [24] on the SAM-FB test set to show the effectiveness of our method. The results in Table 2 show that our method attains the best FID score and the highest CLIP score, illustrating the superiority of our model. We further present our results with different prompts in Table 3, we see that the mask prompt achieves the best results as it provides more accurate position information.

Qualitative Results. We left 3786 images as test split. Figure 4 presents the visualization results on the SAM-FB test set. In each group, the leftmost image depicts the background marked with a position prompt. Our MADD predicts the RGB image and mask of the inserted object, which are shown in the last two images of each group. These

Method	FID↓		CLIP Score↑		MSE↓	
	mask	bbox	mask	bbox	mask	bbox
🟡 [39]	15.41	15.47	0.7079	0.8058	860	883
🟠 [47]	33.68	24.59	–	0.7664	2373	1615
🟢 [29]	–	14.21	–	0.7944	–	830
🟣 [24]	14.49	14.42	0.8014	0.8637	857	845
Ours	13.53	13.60	0.8727	0.8658	760	775

Table 2. Method comparisons on the SAM-FB test set. 🟡 Stable Diffusion, 🟠 PBE, 🟢 GLIGEN, 🟣 Human Affordance.

Prompt	Mask	Bbox	Point	Null	Avg.
FID	13.53	13.60	13.66	13.96	13.69
MSE	760	775	772	860	792
CLIP Score	0.8727	0.8658	0.8567	0.8034	0.8415

Table 3. Comparison of position prompts on the SAM-FB test set.

results demonstrate that MADD not only inserts objects with high quality but also accurately predicts object masks. Figure 1 presents additional results from the SAM-FB test set, illustrating that our model is capable of performing affordance-aware object insertion.

Ablation Study. Table 4 presents the results of our ablation study. We replace the image encoder in the Human Affordance model with DINOv2 as the baseline. Next, we add



Figure 5. We test ambiguous prompts (points and blank) on the in-the-wild images. When providing the prompt of point, 5a, 5b, and 5c show that our model can adjust properties of foreground objects to achieve the affordance insertion. 5d illustrates that the model could find the suitable position to insert the object.

Method	FID (\downarrow)	CLIP $\times 100$ (\uparrow)
Baseline	25.89	89.12
+ Classifier-Free	21.93	91.13
+ Dual diffusion	21.75	91.57
+ Expertise branch	21.55	91.68

Table 4. Ablation study on the SAM-FB test set with 128×128 resolution using mask prompts.

Classifier-Free Guidance to enhance the affordance condition signal. Then we diffuse RGB image and object mask simultaneously, but sharing the entire UNet. Finally, we use two expertise branches for mask and RGB streams. The results show that all of them improved performance.

5.2. Results on In-the-wild Images

Ambiguous Prompts. The training process with position augmentations ensures that the model can understand the affordance relationship between the scene and objects. By using MADD, the model explicitly refines the object’s position, making it capable of handling ambiguous position information. Moreover, the model can adjust the object’s position, size, and view to ensure coherence with the background scene. In Figure 5a, the model adjusts the person’s position around the provided point, placing them on the ground and in front of the bike instead of in the air. Figure 5b demonstrates that the model can change an object’s view. The car’s orientation is adjusted to align with the lane. Figure 5c shows that the model adjusts the size of the coffee beans to match the background scene, even though only a point prompt and a reference image of the statue are provided.

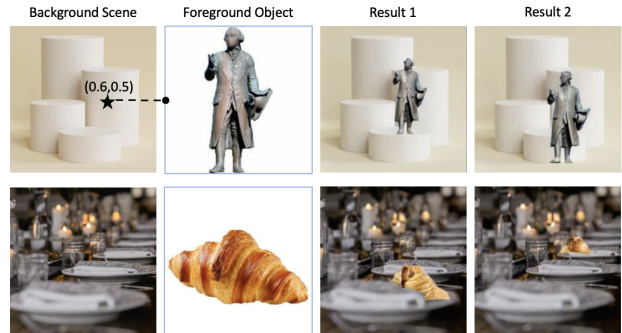
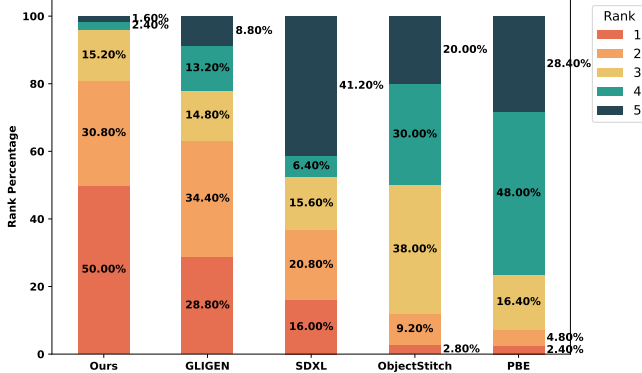


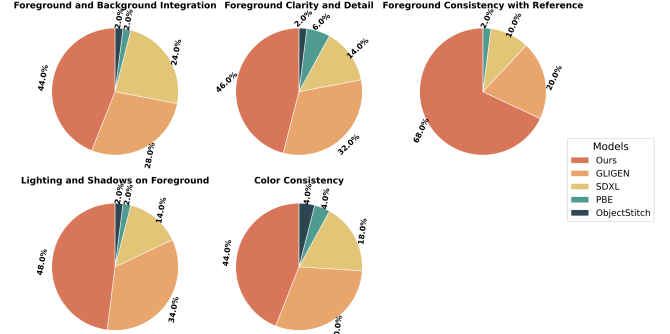
Figure 6. MADD can give different feasible solutions for ambiguous prompts such as point and blank.

vided. Furthermore, the model is capable of placing objects even in the absence of position prompts, as shown in Figure 5d. In this case, the model automatically places the cake onto the plate without any additional clues. When no prompts are provided, the model can still determine a feasible insertion. Additionally, when ambiguous prompts are given, MADD can generate diverse and feasible insertions, as shown in Fig. 6. For a prompt of a point, the model finds reasonable insertions around the point, and for a blank prompt, the model searches for suitable insertions globally.

Human Evaluation. To test the generalization ability of our MADD model, we performed affordance insertion on in-the-wild images and compared the results with Stable Diffusion XL [36], GLI-GEN [29], PBE [47], and Object-Stitch [42]. Instead of merely relying on metrics like FID and CLIP Score, we also conducted a user study to achieve a more comprehensive comparison.



(a) Rank distribution for different methods. Our method has the highest proportion of rank 1 and the least proportion of rank 5.



(b) Rank-1 distribution for each criterion. Each pie chart represents the proportion of times each model achieved Rank-1 for a specific evaluation criterion. Our method dominates every metric.

Figure 7. Human evaluation results on in-the-wild Images. We compared 10 groups of images according to different criteria. Our MADD model outperforms SDXL [39], GLI-GEN [29], ObjectStitch [42] and PBE [47] on overall ranking and each criteria.



Figure 8. MADD can work on images of higher resolution, generating sharper edges, clearer reflections, and improved texture details.

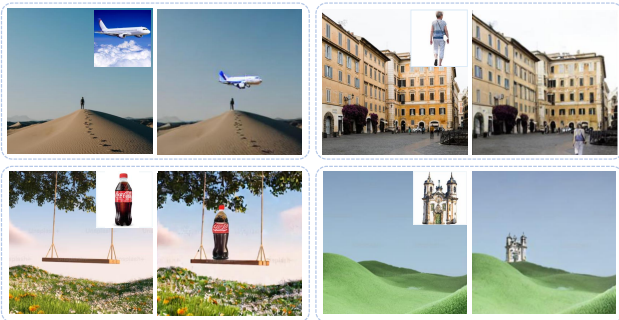


Figure 9. More in-the-wild examples with null prompts. The model can generate an affordance-feasible solution to insert the foreground objects according to the background scene.

We asked 10 users to rank 10 groups of composited images generated by different models according to the following criteria: 1) Foreground and Background Integration,

2) Foreground Clarity and Detail, 3) Foreground Appearance Consistency with Reference, 4) Lighting and Shade on Foreground, 5) Color Consistency.

Figure 7a shows the distribution of ranks for different models, where rank 1 and rank 5 represent the best and worst quality, respectively. Our model achieves 50% of Rank-1 placements and 1.60% of Rank-5 placements, outperforming other methods. Figure 7b provides details for each criterion. Our model consistently achieved the highest proportion of Rank-1 placements across all evaluation criteria, as indicated by the largest segments in each pie chart, especially for maintaining the consistency of foreground appearance with the reference image. This dominance in Rank-1 distribution across multiple criteria highlights the model’s superior performance compared to others in each assessed aspect.

Figure 9 shows additional in-the-wild examples with null

prompts. The results demonstrate the strong generalization ability of our method. The supplementary material contains more samples to further illustrate that our model can provide suitable and diverse solutions in in-the-wild scenarios.

5.3. Results on Higher-Resolution Images

Even though we trained our model at a resolution of 256x256, it is also capable of handling higher-resolution inputs, such as 512x512. To demonstrate this, we fine-tuned our model on SAM-FB at a resolution of 512x512 for only 200 steps and compared it with the original checkpoint on the test split. Figure 8 shows the results of the original checkpoint and the fine-tuned version at higher resolution using the same input. We highlighted the details of the inserted object. It is demonstrated that the model generates sharper edges, clearer reflections, and improved texture details after fine-tuning at a higher resolution.

6. Conclusion

In this paper, we extend the notion of affordance to a more generalized setting, rather than being limited to human-centered tasks. We proposed the affordance-aware object insertion task which involves placing any object into any scene using various types of position prompts. To support this challenging task, we have constructed a SAM-FB dataset which consists of 3,160,403 high-quality foreground-background pairs across over 3,000 object categories. We present a dual-stream diffusion model, **MADD**, which is designed to exploit affordance relationships between foregrounds and backgrounds by simultaneously denoising the foreground appearance and the object mask. Leveraging its understanding of affordance, MADD supports a variety of position prompts, varying from points to masks, and can automatically insert objects even in the absence of explicit prompts. Moreover, MADD exhibits strong generalization capabilities with foreground objects. Our method outperforms previous diffusion-based image composition models on both the SAM-FB test set and in-the-wild images, seamlessly integrating various objects into any background while keeping semantic consistency.

References

- [1] Omri Avrahami, Dani Lischinski, and Ohad Fried. Blended diffusion for text-driven editing of natural images. In *Proceedings of the IEEE/CVF Conference on Computer Vision and Pattern Recognition*, pages 18208–18218, 2022. 3
- [2] Marcelo Bertalmio, Guillermo Sapiro, Vincent Caselles, and Coloma Ballester. Image inpainting. In *Proceedings of the 27th annual conference on Computer graphics and interactive techniques*, pages 417–424, 2000. 3
- [3] Marc H Bornstein. The ecological approach to visual perception, 1980. 2
- [4] Tim Brooks and Alexei A Efros. Hallucinating pose-compatible scenes. In *European Conference on Computer Vision*, pages 510–528. Springer, 2022. 2
- [5] Tim Brooks, Aleksander Holynski, and Alexei A Efros. Instructpix2pix: Learning to follow image editing instructions. In *Proceedings of the IEEE/CVF Conference on Computer Vision and Pattern Recognition*, pages 18392–18402, 2023. 2, 5
- [6] Guillaume Couairon, Jakob Verbeek, Holger Schwenk, and Matthieu Cord. Diffedit: Diffusion-based semantic image editing with mask guidance. *arXiv preprint arXiv:2210.11427*, 2022. 6
- [7] Vincent Delaitre, David F Fouhey, Ivan Laptev, Josef Sivic, Abhinav Gupta, and Alexei A Efros. Scene semantics from long-term observation of people. In *Computer Vision–ECCV 2012: 12th European Conference on Computer Vision, Florence, Italy, October 7–13, 2012, Proceedings, Part VI 12*, pages 284–298. Springer, 2012. 2
- [8] Prafulla Dhariwal and Alexander Nichol. Diffusion models beat gans on image synthesis. *Advances in neural information processing systems*, 34:8780–8794, 2021. 2
- [9] David F Fouhey, Vincent Delaitre, Abhinav Gupta, Alexei A Efros, Ivan Laptev, and Josef Sivic. People watching: Human actions as a cue for single view geometry. In *Computer Vision–ECCV 2012: 12th European Conference on Computer Vision, Florence, Italy, October 7–13, 2012, Proceedings, Part V 12*, pages 732–745. Springer, 2012. 2
- [10] David F Fouhey, Xiaolong Wang, and Abhinav Gupta. In defense of the direct perception of affordances. *arXiv preprint arXiv:1505.01085*, 2015. 2
- [11] Rinon Gal, Yuval Alaluf, Yuval Atzmon, Or Patashnik, Amit H Bermano, Gal Chechik, and Daniel Cohen-Or. An image is worth one word: Personalizing text-to-image generation using textual inversion. *arXiv preprint arXiv:2208.01618*, 2022. 2
- [12] Georgia Gkioxari, Ross Girshick, Piotr Dollár, and Kaiming He. Detecting and recognizing human-object interactions. In *Proceedings of the IEEE conference on computer vision and pattern recognition*, pages 8359–8367, 2018. 2
- [13] Ian Goodfellow, Jean Pouget-Abadie, Mehdi Mirza, Bing Xu, David Warde-Farley, Sherjil Ozair, Aaron Courville, and Yoshua Bengio. Generative adversarial nets. *Advances in neural information processing systems*, 27, 2014. 2
- [14] Abhinav Gupta, Scott Satkin, Alexei A Efros, and Martial Hebert. From 3d scene geometry to human workspace. In *CVPR 2011*, pages 1961–1968. IEEE, 2011. 2
- [15] Kaiming He, Xiangyu Zhang, Shaoqing Ren, and Jian Sun. Deep residual learning for image recognition. In *Proceedings of the IEEE conference on computer vision and pattern recognition*, pages 770–778, 2016. 4
- [16] Jonathan Ho and Tim Salimans. Classifier-free diffusion guidance. *arXiv preprint arXiv:2207.12598*, 2022. 5, 2
- [17] Jonathan Ho, Ajay Jain, and Pieter Abbeel. Denoising diffusion probabilistic models. *Advances in neural information processing systems*, 33:6840–6851, 2020. 4
- [18] Jonathan Ho, Tim Salimans, Alexey Gritsenko, William Chan, Mohammad Norouzi, and David J Fleet. Video dif-

- fusion models. *Advances in Neural Information Processing Systems*, 35:8633–8646, 2022. 3
- [19] Hyeonho Jeong, Gihyun Kwon, and Jong Chul Ye. Zero-shot generation of coherent storybook from plain text story using diffusion models. *arXiv preprint arXiv:2302.03900*, 2023. 6
- [20] Yifan Jiang, Hao Tang, Jen-Hao Rick Chang, Liangchen Song, Zhangyang Wang, and Liangliang Cao. Efficient-3dim: Learning a generalizable single-image novel-view synthesizer in one day. *arXiv preprint arXiv:2310.03015*, 2023. 5
- [21] Tero Karras, Miika Aittala, Janne Hellsten, Samuli Laine, Jaakko Lehtinen, and Timo Aila. Training generative adversarial networks with limited data. *Advances in neural information processing systems*, 33:12104–12114, 2020. 1
- [22] Bahjat Kawar, Shiran Zada, Oran Lang, Omer Tov, Huiwen Chang, Tali Dekel, Inbar Mosseri, and Michal Irani. Imagic: Text-based real image editing with diffusion models. In *Proceedings of the IEEE/CVF Conference on Computer Vision and Pattern Recognition*, pages 6007–6017, 2023. 6
- [23] Alexander Kirillov, Eric Mintun, Nikhila Ravi, Hanzi Mao, Chloe Rolland, Laura Gustafson, Tete Xiao, Spencer Whitehead, Alexander C Berg, Wan-Yen Lo, et al. Segment anything. *arXiv preprint arXiv:2304.02643*, 2023. 2, 3
- [24] Sumith Kulal, Tim Brooks, Alex Aiken, Jiajun Wu, Jimei Yang, Jingwan Lu, Alexei A Efros, and Krishna Kumar Singh. Putting people in their place: Affordance-aware human insertion into scenes. In *Proceedings of the IEEE/CVF Conference on Computer Vision and Pattern Recognition*, pages 17089–17099, 2023. 2, 6, 1
- [25] Sijia Li, Chen Chen, and Haonan Lu. Moecontroller: Instruction-based arbitrary image manipulation with mixture-of-expert controllers. *arXiv preprint arXiv:2309.04372*, 2023. 2
- [26] Tianle Li, Max Ku, Cong Wei, and Wenhui Chen. Dreamedit: Subject-driven image editing. *arXiv preprint arXiv:2306.12624*, 2023. 2, 3
- [27] Wenbo Li, Zhe Lin, Kun Zhou, Lu Qi, Yi Wang, and Jiaya Jia. Mat: Mask-aware transformer for large hole image inpainting. In *Proceedings of the IEEE/CVF conference on computer vision and pattern recognition*, pages 10758–10768, 2022. 3
- [28] Xueting Li, Sifei Liu, Kihwan Kim, Xiaolong Wang, Ming-Hsuan Yang, and Jan Kautz. Putting humans in a scene: Learning affordance in 3d indoor environments. In *Proceedings of the IEEE/CVF Conference on Computer Vision and Pattern Recognition*, pages 12368–12376, 2019. 2
- [29] Yuheng Li, Haotian Liu, Qingyang Wu, Fangzhou Mu, Jianwei Yang, Jianfeng Gao, Chunyuan Li, and Yong Jae Lee. Gligen: Open-set grounded text-to-image generation. In *Proceedings of the IEEE/CVF Conference on Computer Vision and Pattern Recognition*, pages 22511–22521, 2023. 3, 6, 7, 8, 4
- [30] Shilong Liu, Zhaoyang Zeng, Tianhe Ren, Feng Li, Hao Zhang, Jie Yang, Chunyuan Li, Jianwei Yang, Hang Su, Jun Zhu, et al. Grounding dino: Marrying dino with grounded pre-training for open-set object detection. *arXiv preprint arXiv:2303.05499*, 2023. 3
- [31] Xian Liu, Jian Ren, Aliaksandr Siarohin, Ivan Skorokhodov, Yanyu Li, Dahua Lin, Xihui Liu, Ziwei Liu, and Sergey Tulyakov. Hyperhuman: Hyper-realistic human generation with latent structural diffusion. *arXiv preprint arXiv:2310.08579*, 2023. 3, 5
- [32] Lingxiao Lu, Bo Zhang, and Li Niu. Dreamcom: Finetuning text-guided inpainting model for image composition. *arXiv preprint arXiv:2309.15508*, 2023. 3
- [33] Shilin Lu, Yanzhu Liu, and Adams Wai-Kin Kong. Tf-icon: Diffusion-based training-free cross-domain image composition. In *Proceedings of the IEEE/CVF International Conference on Computer Vision*, pages 2294–2305, 2023. 2, 6
- [34] Andreas Lugmayr, Martin Danelljan, Andres Romero, Fisher Yu, Radu Timofte, and Luc Van Gool. Repaint: Inpainting using denoising diffusion probabilistic models. In *Proceedings of the IEEE/CVF Conference on Computer Vision and Pattern Recognition*, pages 11461–11471, 2022. 3
- [35] Maxime Oquab, Timothée Darcet, Théo Moutakanni, Huy Vo, Marc Szafraniec, Vasil Khalidov, Pierre Fernandez, Daniel Haziza, Francisco Massa, Alaaeldin El-Nouby, et al. Dinov2: Learning robust visual features without supervision. *arXiv preprint arXiv:2304.07193*, 2023. 5
- [36] Dustin Podell, Zion English, Kyle Lacey, Andreas Blattmann, Tim Dockhorn, Jonas Müller, Joe Penna, and Robin Rombach. Sdxl: Improving latent diffusion models for high-resolution image synthesis. *arXiv preprint arXiv:2307.01952*, 2023. 7
- [37] Alec Radford, Jong Wook Kim, Chris Hallacy, Aditya Ramesh, Gabriel Goh, Sandhini Agarwal, Girish Sastry, Amanda Askell, Pamela Mishkin, Jack Clark, et al. Learning transferable visual models from natural language supervision. In *International conference on machine learning*, pages 8748–8763. PMLR, 2021. 5
- [38] Tianhe Ren, Shilong Liu, Ailing Zeng, Jing Lin, Kunchang Li, He Cao, Jiayu Chen, Xinyu Huang, Yukang Chen, Feng Yan, et al. Grounded sam: Assembling open-world models for diverse visual tasks. *arXiv preprint arXiv:2401.14159*, 2024. 3
- [39] Robin Rombach, Andreas Blattmann, Dominik Lorenz, Patrick Esser, and Björn Ommer. High-resolution image synthesis with latent diffusion models. In *Proceedings of the IEEE/CVF conference on computer vision and pattern recognition*, pages 10684–10695, 2022. 3, 4, 6, 8
- [40] Nataniel Ruiz, Yuanzhen Li, Varun Jampani, Yael Pritch, Michael Rubinstein, and Kfir Aberman. Dreambooth: Fine tuning text-to-image diffusion models for subject-driven generation. In *Proceedings of the IEEE/CVF Conference on Computer Vision and Pattern Recognition*, pages 22500–22510, 2023. 2
- [41] Jiaming Song, Chenlin Meng, and Stefano Ermon. Denoising diffusion implicit models. *arXiv preprint arXiv:2010.02502*, 2020. 4
- [42] Yizhi Song, Zhifei Zhang, Zhe Lin, Scott Cohen, Brian Price, Jianming Zhang, Soo Ye Kim, and Daniel Aliaga. Object-stitch: Object compositing with diffusion model. In *Proceedings of the IEEE/CVF Conference on Computer Vision and Pattern Recognition*, pages 18310–18319, 2023. 3, 5, 7, 8

- [43] Roman Suvorov, Elizaveta Logacheva, Anton Mashikhin, Anastasia Remizova, Arsenii Ashukha, Aleksei Silvestrov, Naejin Kong, Harshith Goka, Kiwoong Park, and Victor Lempitsky. Resolution-robust large mask inpainting with fourier convolutions. *arXiv preprint arXiv:2109.07161*, 2021. 3
- [44] Brandon Trabucco, Kyle Doherty, Max Gurinas, and Ruslan Salakhutdinov. Effective data augmentation with diffusion models. *arXiv preprint arXiv:2302.07944*, 2023. 3
- [45] Su Wang, Chitwan Saharia, Ceslee Montgomery, Jordi Pont-Tuset, Shai Noy, Stefano Pellegrini, Yasumasa Onoe, Sarah Laszlo, David J Fleet, Radu Soricut, et al. Imagen editor and editbench: Advancing and evaluating text-guided image inpainting. In *Proceedings of the IEEE/CVF conference on computer vision and pattern recognition*, pages 18359–18369, 2023. 2
- [46] Xiaolong Wang, Rohit Girdhar, and Abhinav Gupta. Binge watching: Scaling affordance learning from sitcoms. In *Proceedings of the IEEE Conference on Computer Vision and Pattern Recognition*, pages 2596–2605, 2017. 2
- [47] Binxin Yang, Shuyang Gu, Bo Zhang, Ting Zhang, Xuejin Chen, Xiaoyan Sun, Dong Chen, and Fang Wen. Paint by example: Exemplar-based image editing with diffusion models. In *Proceedings of the IEEE/CVF Conference on Computer Vision and Pattern Recognition*, pages 18381–18391, 2023. 3, 6, 7, 8, 4
- [48] Yifan Yang, Houwen Peng, Yifei Shen, Yuqing Yang, Han Hu, Lili Qiu, Hideki Koike, et al. Imagebrush: Learning visual in-context instructions for exemplar-based image manipulation. *Advances in Neural Information Processing Systems*, 36, 2024. 3
- [49] Bangpeng Yao and Li Fei-Fei. Modeling mutual context of object and human pose in human-object interaction activities. In *2010 IEEE Computer Society Conference on Computer Vision and Pattern Recognition*, pages 17–24. IEEE, 2010. 2
- [50] Jiahui Yu, Zhe Lin, Jimei Yang, Xiaohui Shen, Xin Lu, and Thomas S Huang. Generative image inpainting with contextual attention. In *Proceedings of the IEEE conference on computer vision and pattern recognition*, pages 5505–5514, 2018. 3
- [51] Youcai Zhang, Xinyu Huang, Jinyu Ma, Zhaoyang Li, Zhaochuan Luo, Yanchun Xie, Yuzhuo Qin, Tong Luo, Yaqian Li, Shilong Liu, et al. Recognize anything: A strong image tagging model. *arXiv preprint arXiv:2306.03514*, 2023. 4
- [52] Yuke Zhu, Alireza Fathi, and Li Fei-Fei. Reasoning about object affordances in a knowledge base representation. In *Computer Vision–ECCV 2014: 13th European Conference, Zurich, Switzerland, September 6–12, 2014, Proceedings, Part II 13*, pages 408–424. Springer, 2014. 2

Affordance-Aware Object Insertion via Mask-Aware Dual Diffusion

Supplementary Material

A. More Implementation Details

A.1. SAM-FB Dataset

Figure 11a shows the object masks before and after the data quality control. We see that with our designed data quality control, the foreground object masks have better quality. Figure 11b illustrates the word cloud of our SAM-FB dataset, we observe that our SAM-FB dataset consists of diverse object categories. Table 5 demonstrates the specific threshold for each filter operation of our data quality control stage. With these filter operations, only 0.25% of the masks are left, which ensures the quality of the obtained dataset.

A.2. Training Details

We constructed our dual-stream UNet based on the Stable Diffusion Inpainting v1.5 model, incorporating several modifications. Specifically, we replicated both the first down-sampling block (including `conv_in` and the first Down Block) and the last up-sampling block (including the last Up Block and `conv_out`) to accommodate dual-stream inputs and outputs. To bypass the need to start from scratch, we initialized our model using the pre-trained Stable Diffusion Inpainting v1.5 checkpoint for the unchanged blocks. To optimize our computing resources, we employed a gradual scaling-up approach to train our model. Initially, the model was trained at a resolution of 128×128 , with a batch size of 1024 and a learning rate of 1.25×10^{-4} . This phase included 5,000 warm-up steps, followed by a constant schedule. We then fine-tuned the model at a higher resolution of 256×256 , reducing the batch size to 256 and adjusting the learning rate to 5×10^{-5} . For the diffusion process, the time step is 1000 with a linear noise scheduler. We use 2048 samples of SAM-FB for testing and the rest for training. To ensure a fair comparison with other methods, we re-implemented and re-trained the closest method, Human Affordance, since the authors did not release either the model weights or the full dataset they used. We adopted the diffusion model architecture provided by the authors and trained it using our SAM-FB dataset. Additionally, we replaced the mask input in the original model with our position map to ensure compatibility with the SAM-FB dataset.

A.3. Data Augmentation

To prevent the model from learning a copy-and-paste process, we introduce different augmentations for the background images, foreground images, and position prompts.

Background Augmentation Given that the images in the SA-1B dataset are not square, we rescale and crop them focusing on the objects. Our first step is to resize each source

Filter condition	Threshold	Reserved Percentage
None (Initial)	–	100%
Relative Size	[0.1, 0.75]	7.10%
Aspect Ratio	≤ 3	6.88%
Components Num.	≤ 4	6.71%
Color Std.	≥ 45	1.69%
ResNet50 Score	≥ 0.7	0.25%

Table 5. Reserved percentage for foreground quality control filters. We combine different rule-based and learning-based conditions. Through this process, foreground objects with high quality are reserved.

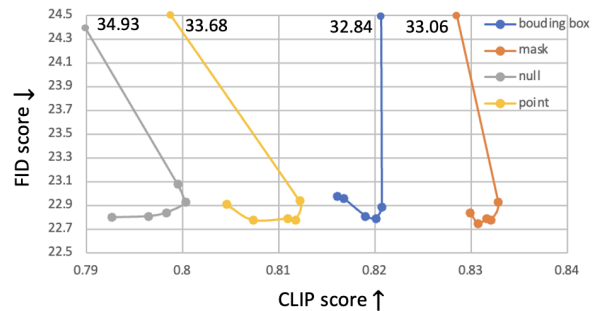


Figure 10. FID-CLIP score curve on 128×128 resolution with different guidance scale [1.0, 3.0, 4.0, 5.0, 6.0, 7.0].

image so that its shorter edge measures 256 pixels. Following this, we randomly center a 256×256 bounding box around each valid object mask, randomly chosen to provide varied backgrounds for the same object. This technique introduces slight background differences for identical objects. Additionally, we allow the bounding boxes to partially crop the objects. This strategy is specifically designed to enable the model to learn from scenarios where objects are partially obscured by the edges of the image.

Foreground Augmentation To prevent the model from simply copying and pasting foreground objects and to increase the diversity of foreground objects, data augmentation is necessary. We used geometric and color augmentations based on Kulal’s work [24] and StyleGAN-ADA [21]. Geometric augmentations included isotropic scaling, rotation, anisotropic scaling, and cutout, each with a probability of 0.4, 0.4, 0.2, and 0.2 respectively. Color augmentations included brightness, contrast, saturation, image-space filtering, and additive noise, each with a probability of 0.2.

Position Prompt Augmentation Our method requires the model to perceptively adjust the position of the inserted ob-

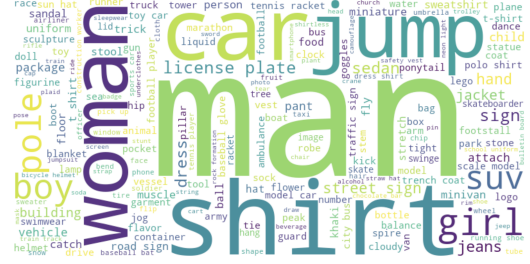


Figure 11. **11a** shows the candidate foreground samples in the pipeline. The upper row shows four low-quality samples. The lower row shows the samples after data quality control. **11b** shows the word cloud of foreground categories in the SAM-FB dataset.

Method	FID↓					CLIP Score $\times 100$ ↑				
	mask	bbox	point	null	Avg.	mask	bbox	point	null	Avg.
Baseline	25.89	26.21	26.37	27.35	26.46	89.12	89.50	79.92	79.31	84.46
+Classifier-Free	21.93	22.03	22.31	22.74	22.25	91.13	90.95	85.49	85.26	88.21
+Dual Diffusion	21.75	21.81	21.90	22.39	21.96	91.57	91.05	88.25	88.34	89.80
+Expertise branch	21.55	21.66	21.76	22.24	21.80	91.68	90.96	89.61	88.30	90.14

Table 6. Experimental results on SAM-FB test set. The difference between the four kinds of prompts indicates that the performance will be better with a more precise position prompt.

ject in response to an ambiguous position prompt; therefore, it is also necessary to augment the position prompts. For points, we perform random jittering to deviate them from their original positions. For bounding boxes, we randomly enlarge each box. We adopt mask enlarging and feathering for mask prompts.

A.4. Classifier Free Guidance

An essential mechanism we employ to support the Null position prompt is Classifier-Free Guidance (CFG). This approach not only enhances the performance of a well-trained Stable Diffusion model but also simplifies handling Null prompts by converting them into Classifier-Free cases. It does this by controlling additional guidance signals each time we sample \mathbf{z}_{t-1} from \mathbf{z}_t and $\hat{\epsilon}_t$.

Ho & Salimans[16] figured out that it is feasible to use the same model to generate an inherent Classifier-Free Guidance signal $p(\mathbf{z}_t|\emptyset)$ as long as we drop certain conditions during the training procedure. Since we have three different conditions \mathbf{f} , \mathbf{b} , and \mathbf{p} , we drop all the conditions with a 0.1 probability and only drop \mathbf{p} with a 0.1 probability. During the inference steps, we can use the CFG to guide the sampling schedule as follows:

$$\hat{\epsilon}_t = (1 + s)\epsilon_{\theta}(\mathbf{z}_t; \mathbf{b}, \mathbf{f}, \mathbf{p}, t) - s\epsilon_{\theta}(\mathbf{z}_t; \emptyset, t) \quad (8)$$

where s is the classifier-free guidance scale.

We test the FID and CLIP scores for different prompts with different guidance scales s . Figure 10 shows the FID-

CLIP curves using different guidance scales ranging from [1.0, 3.0, 4.0, 5.0, 6.0, 7.0]. We set the guidance scale to 4.0 as it usually gives good results across all different prompts.

B. Evaluation

B.1. Evaluation metrics

Our method aims to establish a reasonable relationship between foreground objects and background scenes while maintaining the appearance of the object similar to a reference image and generating a high-quality synthetic image. To assess these two capabilities, we employ two metrics. Firstly, we use the FID score, which is widely used to measure the harmony of images obtained by generative models, to evaluate the quality of synthetic images. We use a pre-trained Inception model to extract features and calculate the FID score between generated images and ground truth images on the SAM-FB test set. Secondly, we evaluate the appearance of the inserted object and the reference foreground image using the CLIP score. We use a CLIP image encoder to extract features. The CLIP score is calculated as the cosine similarity between the two features.

B.2. Human Evaluation

When comparing the results generated by our methods and baseline methods, we asked user to evaluate the quality of the generated image following these five criteria:

- **Foreground and Background Integration:** How natu-



Figure 12. Example of objects with details. Our model could keep the appearance better even with some details compared with SD [39], GLI-GEN [29] and PBE [47]. The first row demonstrates the ability to keep some image texture, and the second row illustrates the ability to keep text texture.

rally does the inserted foreground blend with the background? Does it look out of place or integrate seamlessly?

- **Foreground Clarity and Detail:** Assess the clarity, detail, and resolution of the **inserted foreground**.
- **Foreground Appearance Consistency with Reference:** Check if the inserted foreground’s appearance (shape, texture) matches the foreground in the reference image.
- **Lighting and shade on Foreground:** Evaluate whether highlights and shades on the inserted foreground are realistic and consistent with the background lighting.
- **Color Consistency:** Assess the overall color harmony. Do the inserted foreground and background tones, hues, and saturation levels align?

We conducted our user survey by asking 10 users to rank outputs from different models in 10 affordance insertion settings, therefore gaining 100 data points.

C. More Results

C.1. Details Maintaining

Using DINOv2 features, the model preserves the appearance more effectively than other image editing models, especially for objects with detailed textures. Figure 12 compares our model with other image editing models. Our model demonstrates the ability to retain the details of an object’s appearance, even the texture of the object.

C.2. SAM-FB Test Split

Figure 13 shows a visualization result with different baselines on the SAM-FB test split. Our model generated more authentic results compared to other baseline models.

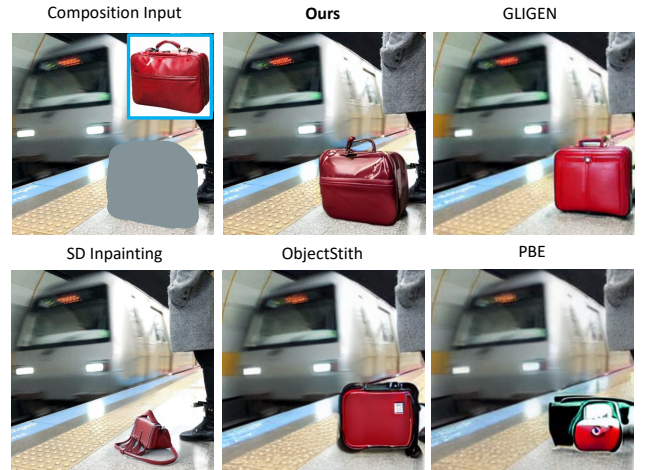


Figure 13. Samples on SAM-FB test split. Our model inserted the bag with an authentic appearance.

C.3. Detailed Ablations

We show the detailed ablation results on different types of position prompts and the result is presented in Table 6. With all the designs, the model achieves the lowest FID score and the highest CLIP score on average.

C.4. In-the-wild Generalization

We compare our methods with other baseline models on in-the-wild images, and Figure 14 shows the visualization results for comparison. In the first five rows, we performed the affordance insertion task providing a bounding box on both common objects like apples and uncommon objects like cruta. Our methods generated the images with the

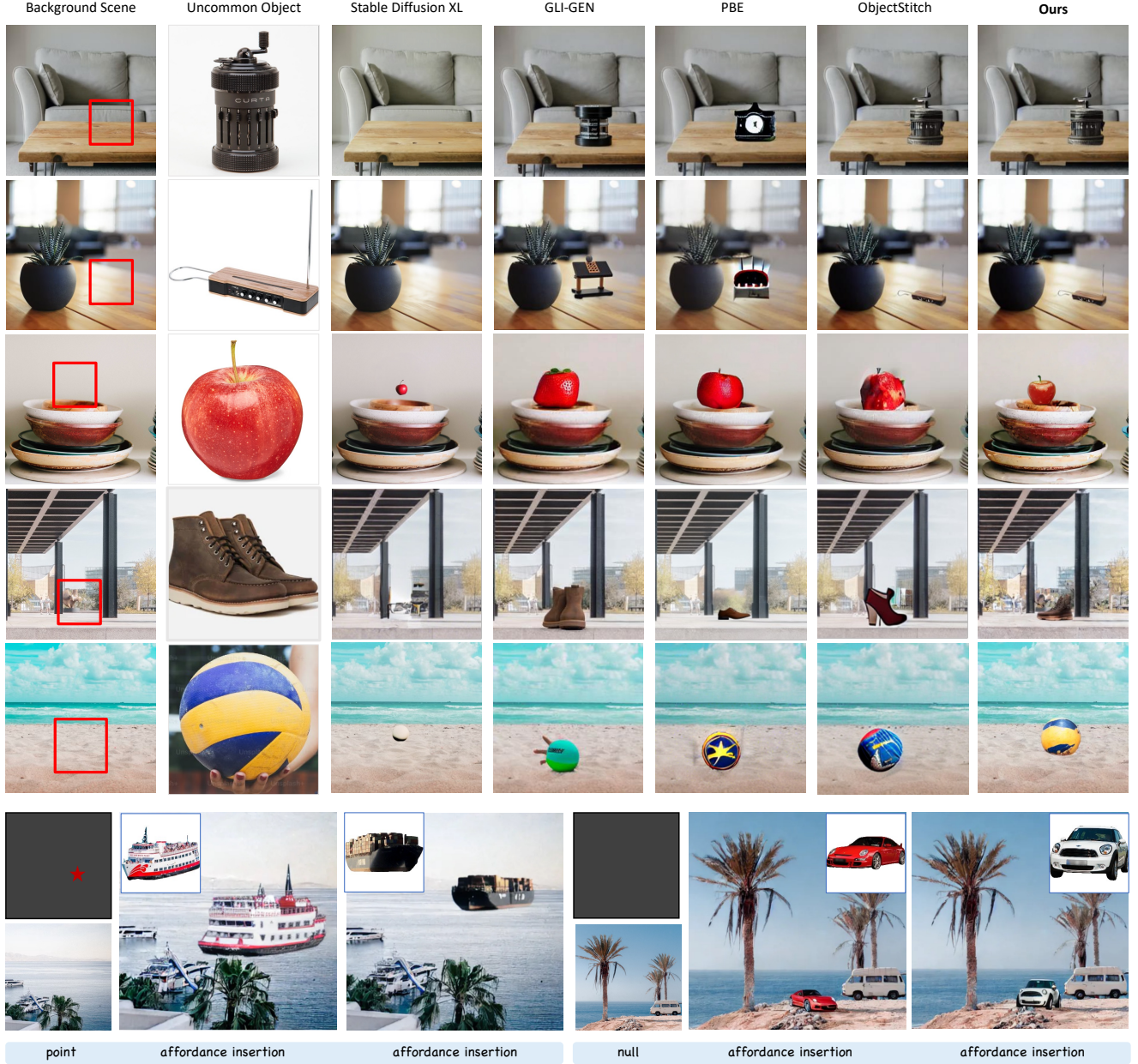


Figure 14. Example of in-the-wild insertion results with details. Our model could keep the appearance better and adjust the foreground’s properties better compared with SD [39], GLI-GEN [29] and PBE [47] on common objects. In the last row, the model generated reasonable insertion when provided with ambiguous prompts.

highest quality, authentic to the reference foreground with proper lighting. In the last row, we show more affordance insertion results when providing ambiguous prompts. The model will automatically find the proper affordance relationship and adjust the location and view of the foreground object. It’s notable that in the first case when inserting the cruise, it is actually the view from the back of the reference image.

C.5. Video Demo

Please refer to the video demo on the project website <https://kakituken.github.io/affordance-any.github.io/>.

C.6. Failure Cases

Figure 15 shows some failure cases when using the model to perform affordance insertion. Generally, when prompted null position, it requires the model to search for

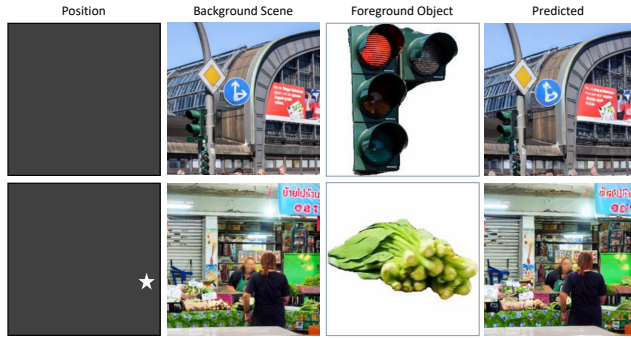


Figure 15. Some failure cases when using our model to perform affordance insertion.

a possible position to insert the object. However, if there are already similar objects in the scene *e.g.*, a traffic light in the first row, it is easy to mislead the model and end up inserting nothing. When the background is too complex and the foreground object is too small, such as a vegetable in a supermarket shown in the second row, it is also difficult for the model to insert the object correctly.